

## Understanding the stability of MnPO<sub>4</sub>

Yiqing Huang,<sup>a</sup> Jin Fang,<sup>a</sup> Fredrick Omenya,<sup>a</sup> Martin O'Shea,<sup>b</sup> Natasha A. Chernova,<sup>a</sup> Ruibo Zhang,<sup>a</sup> Qi Wang,<sup>a,c</sup> Nicholas F. Quackenbush,<sup>d</sup> Louis F. J. Piper,<sup>d</sup> David O. Scanlon,<sup>e,f</sup> and M. Stanley Whittingham<sup>\*a,g</sup>

<sup>a</sup>Chemistry and Material, Binghamton University, Binghamton, NY 13902-6000

<sup>b</sup>SUNY Geneseo, Geneseo, NY 14454

<sup>c</sup>Brookhaven National Lab, Upton NY 11973

<sup>d</sup>Department of Physics, Applied Physics, and Astronomy, Binghamton University, Binghamton New York 13902, USA

<sup>e</sup>University College London, Kathleen Lonsdale Materials Chemistry, Department of Chemistry, 20 Gordon Street, London WC1H 0AJ, UK.

<sup>f</sup>Diamond Light Source Ltd., Diamond House, Harwell Science and Innovation Campus, Didcot, Oxfordshire OX11 0DE, UK.

<sup>g</sup>Northeastern Center for Chemical Energy Storage, Department of Chemistry, Stony Brook University, Stony Brook, NY 11794-3400, USA. \*E-mail: stanwhit@gmail.com

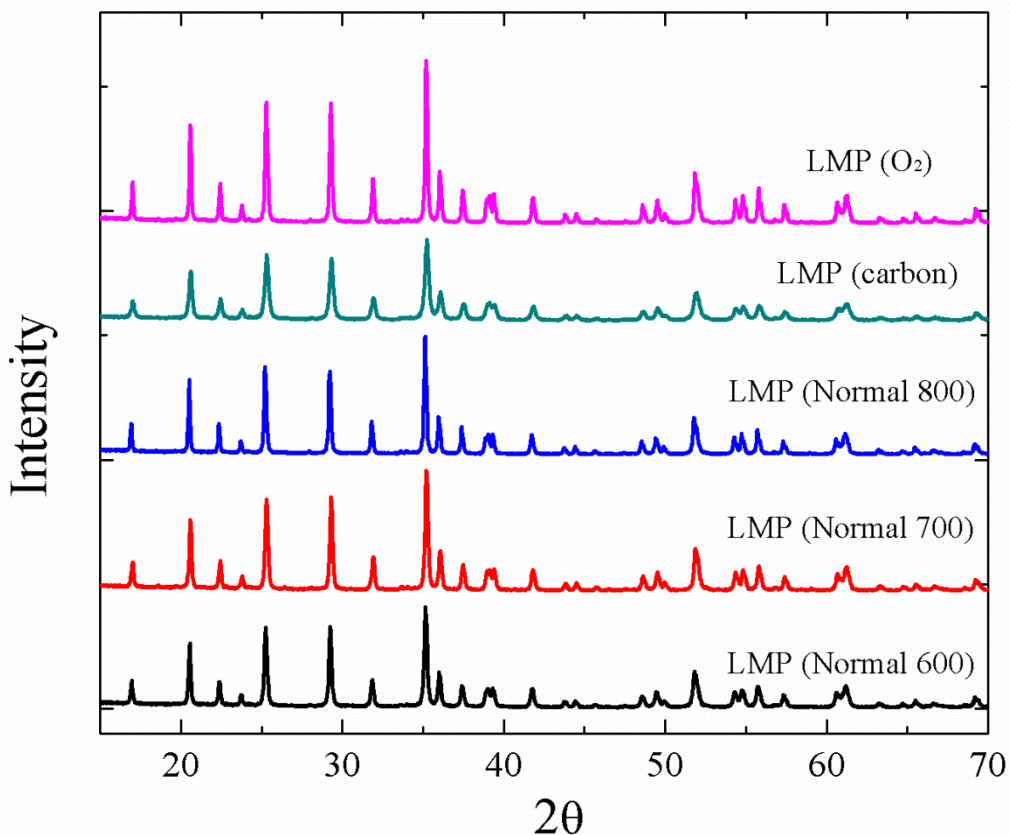


Fig S1: XRD patterns of LiMnPO<sub>4</sub> series.

Table S1: Lattice parameters of LiMnPO<sub>4</sub> series.

LiMnPO <sub>4</sub>	a (Å)	b (Å)	c (Å)	Volume (Å)	R <sub>p</sub>
LMP-RC-600	10.460(1)	6.111(1)	4.750(1)	303.6	6.85
LMP-RC-700	10.457(1)	6.109(1)	4.748(1)	303.3	6.71
LMP-RC-800	10.452(1)	6.107(1)	4.747(1)	303.0	7.98
LMP-CC-700	10.448(1)	6.105(1)	4.748(1)	302.8	6.46
LMP-NC-700	10.448(1)	6.104(1)	4.745(1)	302.6	6.96

Table S2: Elemental analysis and ICP results of LiMnPO<sub>4</sub> series.

Sample	Color	Carbon, wt.%	H, wt.%	ICP ratio
				Li:Mn:P
LMP-RC-600	Grey	0.34	0	1.00:1.03:1
LMP-RC-700	Grey	0.33	0	1.03:1.04:1
LMP-RC-800	Grey	0.23	0	1.04:1.04:1
LMP-CC-700	Black	2.02	0	1.00:1.04:1
LMP-NC-700	White	0	0	1.00:1.03:1

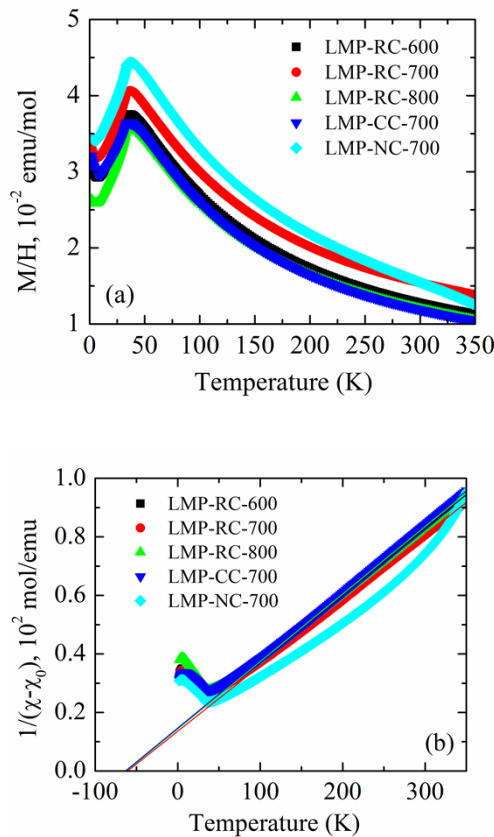


Fig S2: (a) Temperature dependence of the magnetic susceptibility of  $\text{LiMnPO}_4$  series and (b) inverse susceptibilities corrected for temperature-independent contribution and their fit to the Curie-Weiss law.

Table S3: Magnetic parameters of  $\text{LiMnPO}_4$  series.

$\text{LiMnPO}_4$	$\Theta$ (K)	C (emu·K/mol)	$\mu$ ( $\mu_B$ )	$\chi_0$ (emu/mol)	$T_N$ (K)
LMP-RC-600	-63.2	4.375	5.92	$7.4 \cdot 10^{-4}$	33
LMP-RC-700	-60.6	4.473	5.98	$3.0 \cdot 10^{-3}$	33
LMP-RC-800	-62.4	4.338	5.89	0	33
LMP-CC-700	-63.2	4.315	5.88	0	32.5
LMP-NC-700	-	-	-	$2 \cdot 10^{-3}$	33

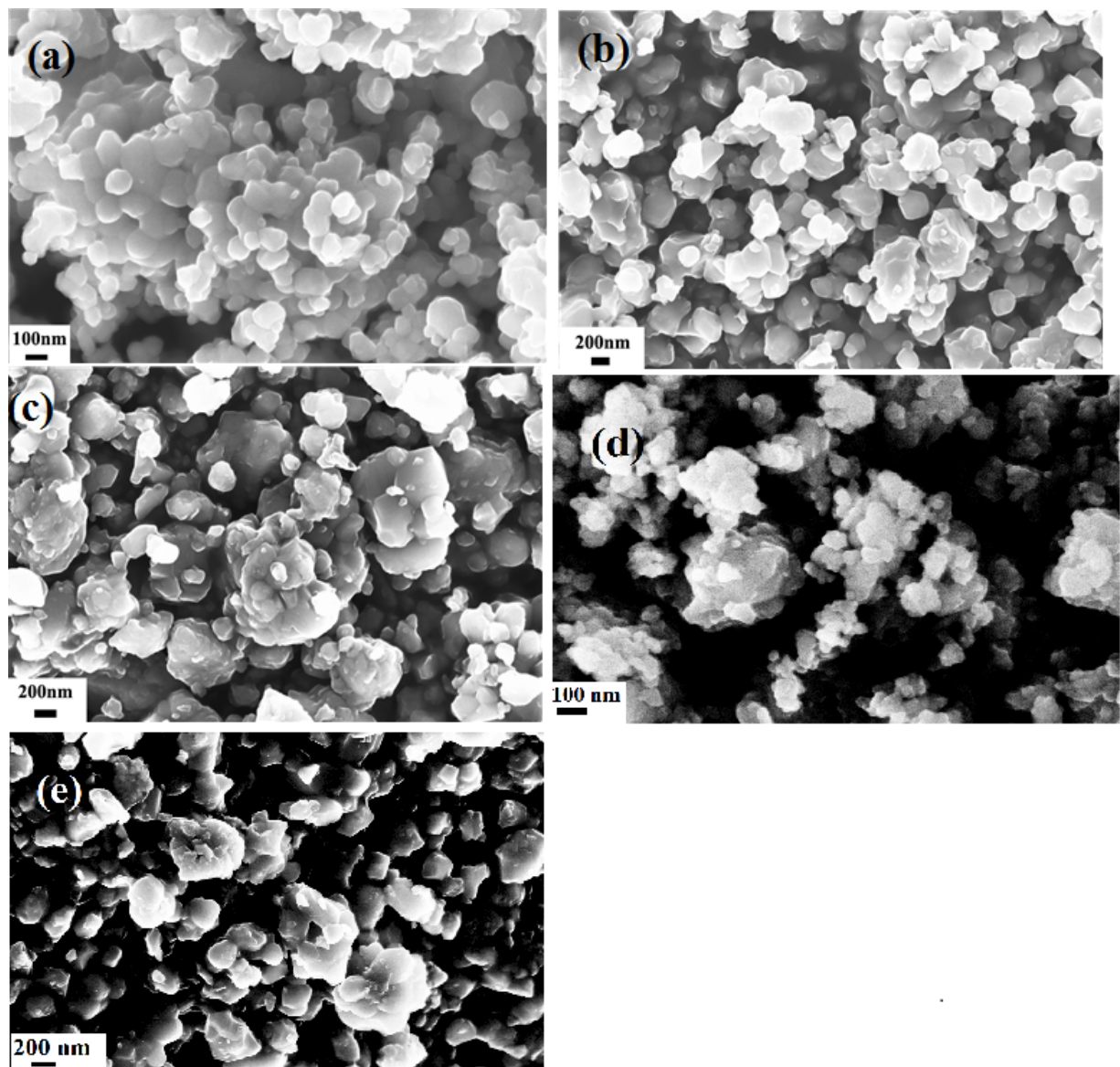


Fig S3: SEM images of (a) LMP-RC-600, (b) LMP-RC-700, (c) LMP-RC-800, (d) LMP-CC-700 and (e) LMP-NC-700.

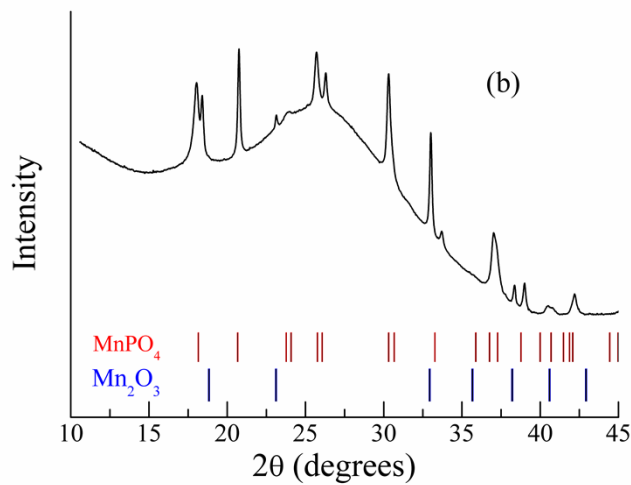
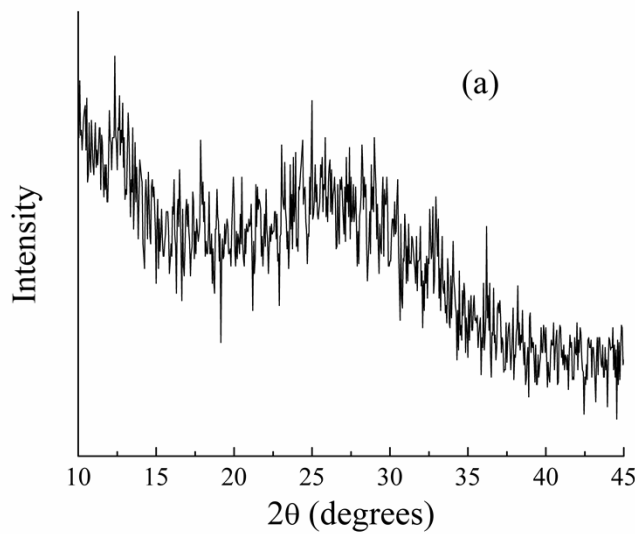


Fig S4: (a) X-ray diffraction pattern of MP-NC-700  $\lambda = 1.54 \text{ \AA}$ , (b) synchrotron X-ray diffraction pattern of MP-NC-700 converted to  $\lambda = 1.54 \text{ \AA}$ .

Using Cu K $\alpha$ , we can hardly see any peak in XRD patterns. But in synchrotron X-ray, some small peaks can be observed, suggesting that the amorphous compound MIGHT consist of MnPO<sub>4</sub> and Mn<sub>2</sub>O<sub>3</sub> (PDF 04-005-4361).

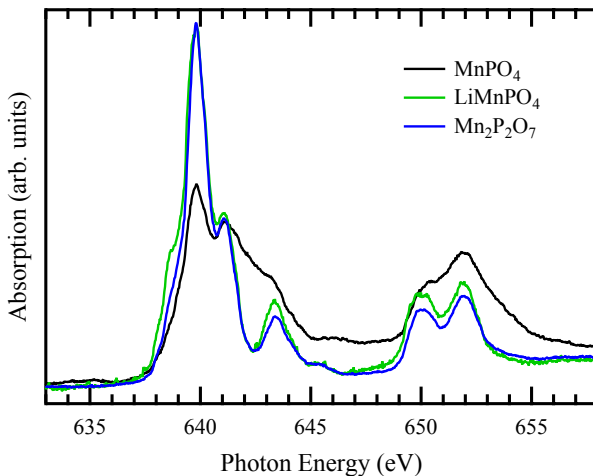


Figure S5: Mn L<sub>3,2</sub>-edge XAS of MnPO<sub>4</sub>, LiMnPO<sub>4</sub>, and Mn<sub>2</sub>P<sub>2</sub>O<sub>7</sub> powders as measured in TEY mode.

Complimentary Mn L<sub>3,2</sub>-edge X-ray absorption spectroscopy measurements were performed at the undulator beamline X1B at the NSLS using the Boston University endstation. The XAS spectra were recorded in both total electron yield (TEY) and total fluorescent yield (TFY) modes with an effective beamline resolution of 0.2 meV. The absorption spectra were normalized to the current from a reference Au-coated mesh in the incident photon beam. The energy scale of the XAS measurements was calibrated using first- and second- order diffraction Ti L<sub>3,2</sub>-edge absorption features of rutile TiO<sub>2</sub>. The XA spectra of the LiMnPO<sub>4</sub> and Mn<sub>2</sub>P<sub>2</sub>O<sub>7</sub> are consistent with spectral line shapes of Mn<sup>2+</sup>, whereas MnPO<sub>4</sub> displays a line shape indicating Mn<sup>3+</sup> in agreement with the literature.<sup>1,2</sup> This reaffirms our assignments of Mn oxidation states in our XPS analysis.

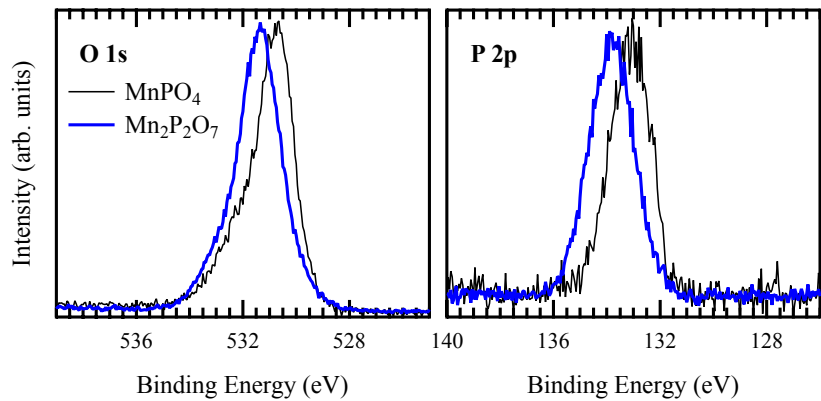


Figure S6: O1s and P 2p core level XPS.

We observe a difference in binding energy of ~0.8 eV between the MnPO<sub>4</sub> and Mn<sub>2</sub>P<sub>2</sub>O<sub>7</sub> in both the O1s and P 2p core level peaks.

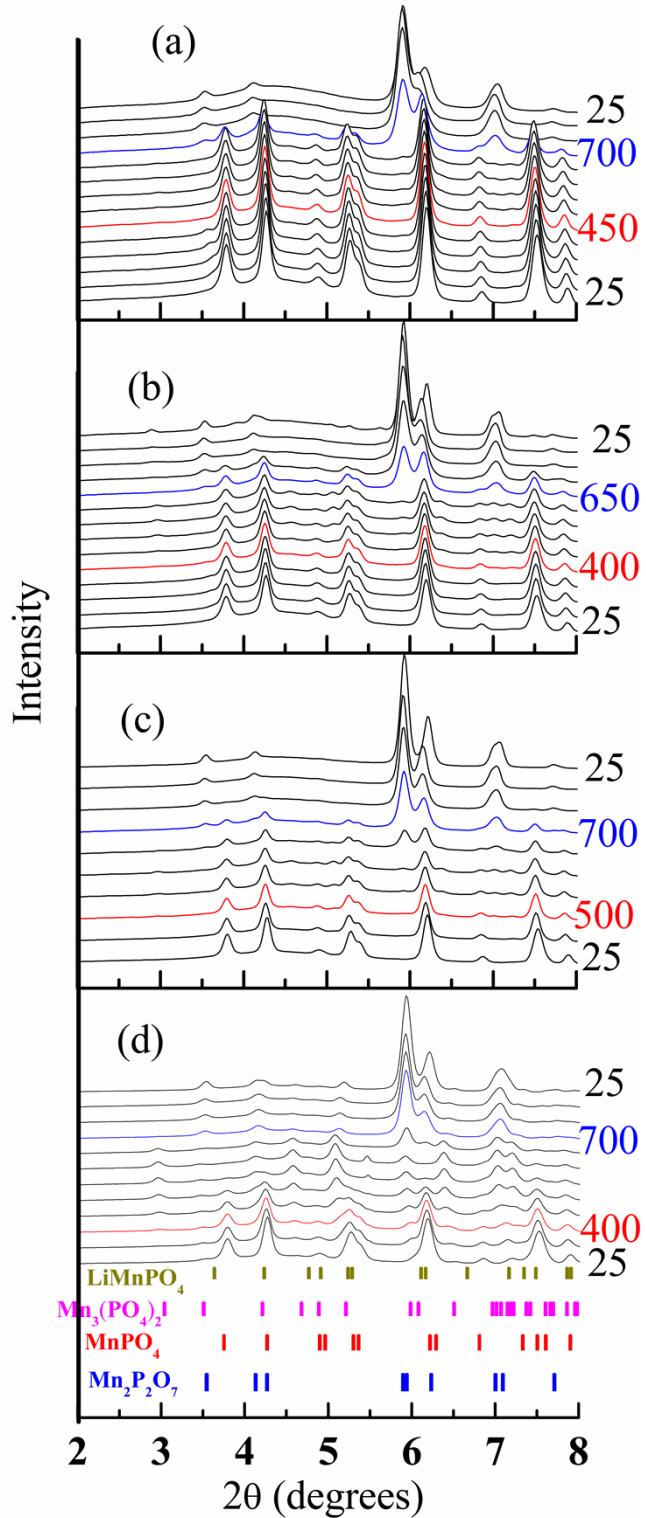


Fig. S7: X-ray diffraction patterns upon heating of MP samples in  $\text{O}_2$ .  $\lambda = 0.3196\text{\AA}$ . Red curves give the temperature where sarcopside  $\text{Mn}_3(\text{PO}_4)_2$  starts to form. Blue curves show the final decomposition temperature.

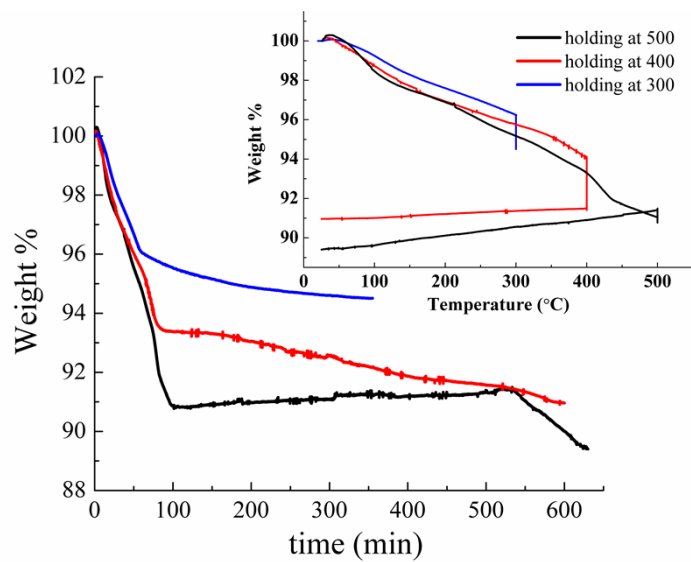


Fig. S8: TGA curves of  $\text{MnPO}_4$  holding at 300, 400 and 500 °C for over 5 hours in ambient atmosphere.

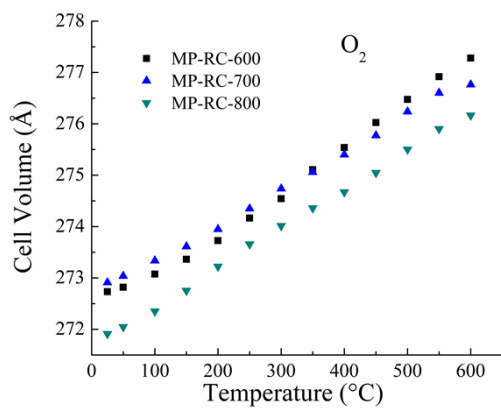
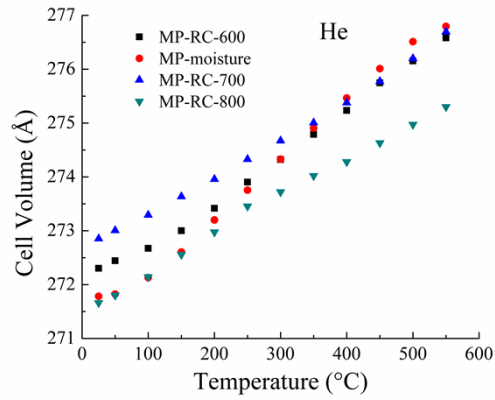


Fig. S9: Unit cell volumes as a function of temperature of  $\text{MnPO}_4$  series in (top)  $\text{N}_2$  and (bottom)  $\text{O}_2$  atmospheres.

References:

1. L. F. J. Piper, N. F. Quackenbush, S. Sallis, D. O. Scanlon, G. W. Watson, K.-W. Nam, X.-Q. Yang, K. E. Smith, F. Omenya, N. A. Chernova, M. S. Whittingham, *J. Phys. Chem. C* 2013, **117**, 10383–10396.
2. L. F. J. Piper, A. R. H. Preston, S. W. Cho, A. DeMasi, B. Chen, J. Laverock, K. E., Smith, L. J. Miara, J. N. Davis, S. N. Basu, U. Pal, S. Gopalan, L. Saraf, T. Kaspar, A. Y., Matsuura, P. A. Glans and J. H. Guo. *J. Electrochem. Soc.*, 2011, **158**, B99.